

**Global potential energy surface, vibrational spectrum, and reaction dynamics of the
first excited (\tilde{A}^2A') state of HO₂**

*Anyang Li and Daiqian Xie**

*Institute of Theoretical and Computational Chemistry, Key Laboratory of Mesoscopic
Chemistry, School of Chemistry and Chemical Engineering, Nanjing University, Nanjing
210093, China*

Richard Dawes and Ahren W. Jasper

Combustion Research Facility, Sandia National Laboratories, Livermore, CA 94551

Jianyi Ma and Hua Guo

*Department of Chemistry and Chemical Biology, University of New Mexico, Albuquerque,
New Mexico 87131*

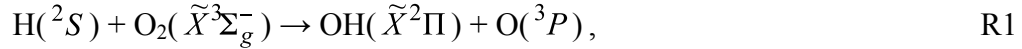
*: corresponding author: dqxie@nju.edu.cn

Abstract

The authors report extensive high-level *ab initio* studies of the first excited (\tilde{A}^2A') state of HO₂. A global potential energy surface was developed by spline fitting 17000 *ab initio* points at the internal contracted multireference configuration interaction (icMRCI) level with the AVQZ basis set. The near-equilibrium region of the potential was also investigated using several dynamically weighted MRCI methods in the complete basis set limit. Vibrational energy levels on both surfaces agree well with each other and a new assignment of some vibrational features is proposed. In addition, the dynamics of both the forward and reverse directions of the H + O₂($\tilde{a}^1\Delta_g$) \leftrightarrow OH + O reaction ($J=0$) were studied using an exact wave packet method. The reactions are found to be dominated by sharp resonances.

I. Introduction

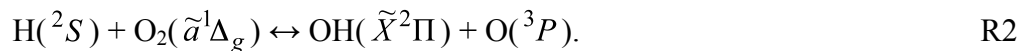
The hydroperoxyl radical (HO_2) is an important transient species in combustion¹ and atmospheric processes.² Formed as the reaction intermediate of the “single most important combustion reaction”,¹ namely



HO_2 provides a diagnostic probe of the flame dynamics and kinetics. The detection of this key intermediate in flames is typically done by IR absorption spectroscopy by exciting the fundamental and overtone vibrational modes of $\text{HO}_2(\tilde{X}^2A'')$.³⁻⁵ It can also be detected⁶ by electronic spectroscopy based on the $\tilde{A} \leftarrow \tilde{X}$ transitions starting at $\sim 7000 \text{ cm}^{-1}$.⁷⁻¹⁰

The first excited \tilde{A}^2A' state of HO_2 is degenerate with the ground \tilde{X}^2A'' state at linearity via the Renner-Teller interaction,¹¹ which is a non-Born-Oppenheimer effect for $J>0$. Both states are strongly bent, and the transition between the two is in the near infrared region. The $\tilde{A} - \tilde{X}$ absorption/emission spectra have been investigated theoretically on semi-global potential energy surfaces (PESs) for the two states.¹²⁻¹⁵ These studies successfully reproduced the high-resolution spectroscopic data of Fink and Ramsey,^{10, 16} shedding valuable light on the ro-vibrational dynamics and the influence of the Renner-Teller coupling.

The excited \tilde{A}^2A' state is also responsible for the reaction:



The forward reaction produces the same product as in R1. The two reactions may scramble via the aforementioned Renner-Teller interaction in the HO₂ complex or via non-adiabatic couplings in the asymptotic OH + O channel.¹⁷ Indeed, such involvements of the \tilde{A}^2A' state in R1 have been speculated in recent experimental¹⁸⁻¹⁹ and theoretical studies.²⁰⁻²³ Obviously, these possibilities are amenable to dynamic studies only when the PESs and their couplings can be accurately determined. In addition, the reverse reaction of R2 might be involved, along with R1, in vibrational relaxation of OH when it collides with O.²⁴ Due to the formation of the HO₂ intermediate, vibrationally inelastic scattering has a large cross section.²⁵ So far, this possibility has only been examined within a statistical model,²⁶ due partly to the lack of a global PES.

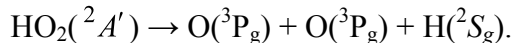
It is clear that a better understanding of the HO₂ system, particularly at higher energies, cannot be achieved without an accurate description of the excited state PES. An earlier attempt to map out the PES of the excited \tilde{A}^2A' state of HO₂ is by Kendrick and Pack,²⁷ who expressed the PES in terms of the DIM (diatom-in-molecule) representation and fitted to a small number of *ab initio* points. The later \tilde{A}^2A' state PESs developed for spectroscopic studies are highly accurate,¹³⁻¹⁴ but they do not extend to dissociation limits and as a result unsuitable for studying reaction dynamics. More recently, Kłos et al. have also reported high-level *ab initio* calculations of the \tilde{A}^2A' state PES in the asymptotic regions.²⁶ In this publication, we report the first globally accurate PES for the \tilde{A}^2A' state, using icMRCI with a larger active space than that reported in our earlier work on the ground state HO₂.²⁸ In addition, we also investigated the near equilibrium region

using a recently developed dynamically weighted MRCI method. To verify the accuracy of these PESs, we have carried out variational calculations of low-lying vibrational levels and compare them with experimental data. In addition, we have also performed scattering calculations for both the forward and reversed reactions of R2 with zero total angular momentum. This publication is organized as follows. The next section (Sec. II) describes theoretical methods. The results are presented and discussed in Sec. III. The final section (Sec. IV) summarizes.

II. Methods

A. *Ab initio* calculations

Here we describe the electronic structure relevant to a global adiabatic description of the first excited electronic state of HO₂. For a consistent notation we use the C_s point group for all structures including those with higher symmetries. There are three distinct dissociation asymptotes each with different electronic state degeneracy patterns (O₂ + H, OH + O, and O + O + H). Consider first building a set of molecular electronic states from separate ground state atoms:



According to Herzberg,²⁹ P_g correlates to (A' + 2 A''), and S_g correlates to A' with all three atoms combining to give (5 A' + 4 A''). The vector addition of spins (two triplets and one doublet) gives one set of sextet, and two sets each of quartet and doublet states. Considering only the doublet states there is therefore a separate atoms asymptotic 18 fold

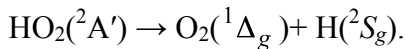
degeneracy ($10 A'$, $8 A''$). Thus the complete dissociation of $\text{HO}_2(1^2 A')$ is to ground state separated atoms and a balanced description of the asymptote requires at least 18 states.

Next we consider loss of an oxygen atom to form ground state products:



Again using Herzberg's tables, we find that the ground Π -state of OH correlates to one A' state and one A'' state, combining with the ($A' + 2 A''$) states from the oxygen atom to give one set ($3 A' + 3 A''$) of doublet states. Thus the first excited state of HO_2 is one of six doublet molecular states that correlate adiabatically to these ground state products.

Finally we consider loss of the hydrogen atom to form molecular oxygen and atomic hydrogen. Ground state $\text{H}(^2 S_g)$ correlates to A' and ground state molecular oxygen $\text{O}_2(^3 \Sigma_g^-)$ correlates to A'' , combining to give just one A'' doublet state. Thus this dissociation channel does not form ground state products, but rather:



The excited state of molecular oxygen ($^1 \Delta_g$) resolves to ($A' + A''$). At this asymptote the pair of states ($A' + A''$) corresponding to excited molecular oxygen lies above the lone A'' state corresponding to ground state products. Adiabatic dissociation of H beginning in the molecular region in a linear configuration starts out with Renner-Teller degeneracy of the ground $1 A''$ state and the excited $1 A'$ state. As the O-H bond is

stretched (maintaining a linear arrangement), a conical intersection (CI) of the $1 A''$ and $2 A''$ states occurs. After the intersection between the two A'' states, the Renner-Teller degeneracy of the A' state switches from the $1 A''$ to the $2 A''$ state arriving asymptotically to the $(A' + A'')$ pair corresponding to the excited state of molecular oxygen ($^1\Delta_g$).

In this work, we report two sets of *ab initio* calculations of the excited state of HO₂, using the MOLPRO package.³⁰ In the first approach, three fitted PESs (differing in the details of the *ab initio* methods employed) were constructed for the excited $^2 A'$ state of HO₂ using an automated interpolating moving least-squares (IMLS) based scheme.³¹⁻³² *Ab initio* energies were calculated at approximately 1500 automatically determined geometries to generate each PES. Jacobi coordinates were used with ranges of $r_{OO} = [1.0, 2.1]$ Å, and $R_{H-OO} = [0.5, 2.65]$ Å. Data was only computed for $\theta \leq \pi/2$ with the symmetry partner ($\pi-\theta$) added at no cost. Energy was restricted to a range of 70 kcal/mol. Based on considerations described above, a total of 18 doublet electronic states ($10 A'$, $8 A''$) were included in generalized dynamically weighted state averaged complete active space self-consistent field (GDW-SA-CASSCF) calculations³³⁻³⁴ using a full-valence active space. Maximum weight was focused on the A' state of interest, and weights for other states were determined by the GDW scheme. As has been discussed previously,³³⁻³⁴ the weights obtained by this scheme smoothly connect the various asymptotes and properly reflect differing degeneracies (asymptotic as well as Renner-Teller). Three PESs were

constructed using different approaches for including dynamic electron correlation. For the first PES (PES1-1), the GDW-SA-CASSCF method was used as the reference for subsequent MRCI+Q calculations.³⁵⁻³⁷ The CBS limit for valence electron correlation was estimated from two zeta levels using the l^3 formula³⁸ and the Dunning aug-cc-pVTZ and aug-cc-pVQZ basis sets.³⁹ Two other PESs were constructed using CBS extrapolation and the ACPF method.⁴⁰ To assess the importance of core-valence correlation effects, separate PESs were constructed, first correlating only the valence electrons (PES1-2) and then all electrons (PES1-3). The ACPF method is known to be unreliable for excited states, but was tested here given that the excited state of HO₂ of interest is the lowest A' state, and the method has good size-extensivity making it useful for core-valence corrections.

For the global PES, denoted as PES2, *ab initio* electronic energies of the lowest excited state of HO₂(\tilde{A}^2A') were calculated using the MRCI+Q method.³⁵⁻³⁷ The aug-cc-pVQZ basis set³⁹ generated a total of 206 Gaussian-type orbitals (GTOs). The state-averaged complete active space self-consistent field (CASSCF) calculations for equally weighted $1^2A''$ and $1^2A'$ states have been carried out with the full valence active space (13 active electrons in 9 active orbitals), while the 1s orbitals of the oxygen atoms were kept doubly occupied but fully optimized. This active space is significantly larger than that used in our earlier work, which included 9 active electrons in 7 active orbitals.^{28, 41} Based on the CASSCF natural orbitals, icMRCI+Q calculations were carried

out with all the CAS-configurations as the reference configuration state functions. In order to include core-valence and core-core correlations, the $1 a'$ and $2 a'$ orbitals, which are primarily composed of the oxygen $1s$ orbitals and were frozen in our earlier work,^{28, 41} were also correlated through single and double excitations. The total number of contracted configurations in the present calculations was about 3.2×10^6 , which is much larger than that used in our earlier work on the ground state PES (1.2×10^6).^{28, 41} All calculations were performed in C_s symmetry.

It is useful to label the two oxygen atoms as O_1 and O_2 , and the global PES was constructed in the term of internal coordinates $(r_{O_1H}, r_{O_1O_2}, \theta)$, where r_{O_1H} is the distance between the H atom and one O atom, $r_{O_1O_2}$ is the distance between the two O atoms, and θ is the enclosed bond angle. We chose relatively dense grids for the two radial coordinates with 28 points covering the O–O radial coordinate from 1.8 to $20.0 a_0$, and 31 points in the O–H radial coordinate from 1.2 to $15.0 a_0$. In the angular coordinate, 19-25 points ranging from 0° to 180° were used. Thus this gives about 17000 symmetry-unique points. Finally, a three-dimensional cubic spline interpolation was employed to yield a global PES for the system.

In addition to the excited PES, the ground state PES of HO_2 was also updated at the same level of theory. Instead of recalculating all the points, we used the “hierarchical construction” (HC) scheme,⁴² in which the high accuracy PES was written as a sum of a PES based on dense but low accuracy *ab initio* points and an additional function fitted to

the difference between high and low accuracy *ab initio* points on a sparse grid. For the low accuracy PES, we used the XXZLG potential,^{28,41} which included more than 18000 *ab initio* points. For the high accuracy method, we have chosen the same method described above for the excited state PES of HO₂. 4000 points were used to fit the difference PES.

B. Vibrational spectrum calculations

The Hamiltonian with the total angular momentum $J=0$ can be written in Jacobi coordinates (R, r, γ) as

$$\hat{H} = -\frac{1}{2\mu_R} \frac{\partial^2}{\partial R^2} - \frac{1}{2\mu_r} \frac{\partial^2}{\partial r^2} + \frac{\hat{j}^2}{2\mu_r r^2} + \frac{\hat{j}^2}{2\mu_R R^2} + V(R, r, \gamma). \quad (1)$$

In the vibrational calculations, R is defined the distance from H to the center of mass of the O₂ fragment, r is the internuclear distance of O–O, and γ is the angle between R and r . μ_R and μ_r are the reduced masses of H–O₂ and O₂, respectively. \hat{j}^2 is the diatom rotational angular momentum operator. The last term in Eq. (1) represents the excited state PES for HO₂(\tilde{A}^2A'). No Renner-Teller term was included as the low-lying vibrational levels are far from linearity.

The radial Jacobi coordinate R was represented by 70 potential-optimized discrete variable representation⁴³⁻⁴⁴ (PODVR) points derived from the one-dimensional Hamiltonian, in which the two other coordinates were fixed at their equilibrium values. The other radial coordinate r was also represented by 50 PODVR points from the

corresponding one-dimensional Hamiltonian. For the angular variable, a 25-point Gauss–Legendre grid⁴⁵ was chosen between 0-90°. Because only the vibrational states corresponding to the odd O–O exchange parity are of interest, half of the DVR points in the angular coordinate were discarded. Due to nuclear spin statistics, the permutation symmetry for the two oxygen atoms in HO₂(\tilde{A}^2A') should be even. The symmetry adaption thus includes only the even Legendre polynomials and only half of the DVR grid in the angular coordinate. The vibrational energy levels were calculated using the Lanczos method⁴⁶ which generated the eigenvalues of the Hamiltonian by a three-term recursion. With a cutoff of 6 eV for the potential energy, about 3000 Lanczos recursion steps were carried out to generate the converged vibrational energy levels. When eigenfunctions were required, the Lanczos recursion was repeated to assemble the wave functions of interest.

C. Reaction dynamics

The scattering calculations were performed using a state-to-state wave packet method based on the Chebyshev propagator,⁴⁷⁻⁴⁸ which is generally more accurate and efficient than the time propagator.⁴⁹⁻⁵⁰ Essentially, an internal state specific Gaussian wave packet was launched in the reactant channel, and propagated using the three-term recursion relation for Chebyshev polynomials. The projection of the final states was carried out in the product channel, using a coordinate transform scheme.^{48, 51} Damping functions were imposed in the asymptotes to enforce the outgoing wave boundary

conditions.⁵²

In this work, we restrict our attention to the $J=0$ reaction probabilities for both the forward and reverse reactions in R2. The Hamiltonian is the same as in Eq. (1), but the Jacobi coordinates are defined differently for the two reactions. For the $\text{H} + \text{O}_2$ reaction, the same Jacobi coordinates as used in the vibrational spectrum calculations were used. Symmetry adaptation allowed only the even O_2 rotational levels. For the $\text{OH} + \text{O}$ reaction, on the other hand, the radial coordinates r and R are defined as the O-H and O-OH distances, respectively. In this case, we also consider only the symmetric case for the O-O exchange. The parameters used in the calculations are listed in Table I.

III. Results

A. Potential energy surfaces

The global topography of the new PES for the ground state of $\text{HO}_2(\tilde{X}^2A'')$ is essentially the same as the original XXZLG PES,²⁸ and thus not shown here. However, the large active space in the present calculations improves the energetics. As shown in Table II, the calculated dissociation energies including zero-point energy corrections, $D_0(\text{O-OH})$, is found to be 63.56 kcal/mol, which is only 0.67 kcal/mol lower than the recently recommended experiment value of 64.23 ± 0.08 kcal/mol.⁵³ On the other hand, the calculated exothermicity of 15.90 kcal/mol for the reverse R1 reaction is less than 0.5 kcal/mol lower than the experimental value of 16.24 kcal/mol.⁵³

Table II also presents the equilibrium geometry and dissociation energies for the

excited state $\text{HO}_2(\tilde{A}^2A')$. The calculated equilibrium geometry is located at $r_{\text{OH}}=1.823 a_0$, $r_{\text{OO}}=2.634 a_0$, and $\theta=102.06^\circ$ for PES1-1, and $r_{\text{OH}}=1.827 a_0$, $r_{\text{OO}}=2.642 a_0$, and $\theta=101.80^\circ$ for PES2. These values are very close to the recent theoretical data of Melnikov et al.,¹⁴ which are $r_{\text{OH}}=1.828 a_0$, $r_{\text{OO}}=2.643 a_0$, and $\theta=101.81^\circ$. PES1-1 includes CBS extrapolation of the valence correlation energy, but not core-correlation, while PES2 correlates all electrons, but without CBS extrapolation. The two ACPF surfaces (PES1-2 and PES1-3) shed more light on the importance of core-correlation as they both use CBS extrapolation with PES1-3 also adding core-correlation. Comparing PES1-2 and PES1-3 in Table II, the effect of core-correlation is quite significant, particularly for r_{OH} and θ where the equilibrium angle changes by more than a degree with the addition of core-correlation. This improves the equilibrium geometry on PES1-3 bringing it into very close agreement with the experimental data of Tuckett et al. However, there are some large deviations in the experimental data from different sources shown in Table II. In general the theoretical equilibrium geometries seem to agree better with the work of Tuckett et al.,⁵⁴ rather than the more recent work of Fink and Ramsay.¹⁶

The calculated dissociation energies for $D_e(\text{H-OO})$ and $D_e(\text{O-OH})$ on PES2 are 56.20 and 46.35 kcal/mol, respectively. The zero-point energy corrected values, $D_0(\text{H-OO})$ and $D_0(\text{O-OH})$, are 50.18 and 43.51 kcal/mol, respectively, which are in good agreement with the experimental values of 50.39 and 44.13 kcal/mol, derived from the ground state data and the vertical transition energies for HO_2 (Ref. ¹⁰) and O_2 .²⁹ The calculated

endothermicity of 6.67 kcal/mol for reaction R2 is only about 0.41 kcal/mol higher than the experimental value of 6.26 kcal/mol.

PES2 is displayed in Fig. 1 using the internal coordinates. The upper panel shows the PES as a function of the two bond lengths with the bond angle fixed at its equilibrium value of 101.8° , while the lower panel displays the variation in the r_{OO} and θ coordinates with the O–H bond length fixed at its equilibrium value of $1.827a_0$. The bent potential minimum is clearly shown in the figure.

Figure 2 shows the long-range behaviors of PES2 in the two dissociation channels. The upper panel displays the contour plot for the O+OH channel in the corresponding Jacobi coordinates, where r is the OH internuclear separation (fixed at its equilibrium $1.83 a_0$), R is the distance between the O atom and the center of mass of OH, and γ is the angle between r and R with $\gamma=0^\circ$ for the OH–O collinear arrangement. There is a very shallow well with a depth of 0.087 eV relative to the O+OH dissociation limit, located at $R=5.821 a_0$ corresponding to a hydrogen-bonded OH–O complex. This well is connected to the chemical well via a submerged barrier located at $R=5.258 a_0$, $r=1.834 a_0$, and $\gamma=97^\circ$. In the lower panel of Figure 2, the Jacobi coordinates of the H+O₂ system are used, where r is the O–O internuclear distance, R is the distance between the H atom and the center of mass of O₂, and γ is the angle between r and R . The contour plot of the PES for the $\text{H}(^2S)+\text{O}_2(\tilde{a}^1\Delta_g)$ channel is shown as a function of R and γ for r fixed at the equilibrium value $r_e=2.3 a_0$ for the $\text{O}_2(\tilde{a}^1\Delta_g)$ molecule. It can be seen that an obvious

barrier located at $R=3.774 a_0$, $r=2.304 a_0$, and $\gamma=90^\circ$. And there is a very shallow well (not visible here) corresponding to a linear van der Waals H-O₂ structure at $R=5.035 a_0$. Table III summarizes all the four stationary points mentioned above in internal coordinates. These long-range potentials are very similar to those reported earlier by Kłos et al.²⁶

In Figure 3, the minimal energy paths for the two dissociation channels are displayed. As expected, the \tilde{X}^2A'' and \tilde{A}^2A' states are degenerate in the OH + O asymptote. The shallow wells corresponding to the hydrogen bond complexes and the submerged barriers are clearly seen. On the H + O₂ side, the \tilde{A}^2A' state is asymptotically higher than the \tilde{X}^2A'' state. The ~ 0.25 eV barrier on the excited state PES is clearly seen, while the ground state is barrierless.

B. Vibrational Spectrum of HO₂(\tilde{A}^2A')

In this work, we focus on low-lying vibrational states of HO₂(\tilde{A}^2A'). Table IV lists some of the calculated vibrational energy levels for total angular momentum $J=0$ and even O–O exchange symmetry, obtained from the two PESs. The energy levels are labeled with three vibrational quantum numbers (n_1 , n_2 , and n_3), representing the OH stretching, HOO bending, and O₂ stretching modes, respectively. Some of the vibrational eigenfunctions in the $(0, n_2, 0)$, $(1, \tilde{n}_2, 0)$, and $(0, 0, n_3)$ series are plotted in Fig. 4 in Jacobi coordinates. It is clear that the wave functions of low-lying bound states can be easily assigned and the local mode characters are evident.

It is difficult to record the excited state vibrational spectrum experimentally and thus far only a limited number of measurements have been reported. The currently accepted fundamental frequency for the O-O stretching mode ν_3 (929.068 cm^{-1}) differs considerably from a previously reported value for the band origin of 984.8 cm^{-1} . As shown in Table IV, the calculations for this mode ($\nu_3 = 932.21$ on PES1-1 and 927.95 cm^{-1} on PES2) are in excellent agreement with the more recent value⁵⁵ as well as the calculated results on the PES of Melnikov *et al.*¹⁴ However, the calculated fundamental frequencies for the other two modes ($\nu_1 = 3579.71$ cm^{-1} and $\nu_2 = 1228.55$ cm^{-1} on PES1-1 and $\nu_1 = 3566.72$ cm^{-1} and $\nu_2 = 1196.22$ cm^{-1} on PES2) are much different from the experimental values assigned by Jacox,⁵⁵ namely 3268.5 and 1285 cm^{-1} , respectively. These frequencies were derived by Tuckett *et al.* from the low resolution emission and absorption experiment,⁹ which also gave the old value for $\nu_3 = 984.8$ cm^{-1} . The latter frequency has been questioned by Holstein *et al.*,⁵⁶ casting doubt on the reliability of all the frequencies. The discrepancy between values for ν_1 calculated by the four high-level methods used in this study and experiment of about 300 cm^{-1} strongly suggests misinterpretation of the experimental data. The methods employed in this study have previously proven to be very accurate for calculation of vibrational states in systems with strong multireference character including vibrational levels on high-lying excited electronic states.(refs 32,34)

As shown in Table IV, the four *ab initio* PESs have yielded very similar results for

the ν_1 and ν_2 frequencies. We thus conclude that the two frequencies listed in the Jacox table for $\text{HO}_2(\tilde{A}^2A')$ are incorrect and need to be updated.

C. Reaction dynamics

In Figure 5, the $J=0$ total reaction probabilities for both the forward and reverse R2 reactions are displayed. Both reactions are dominated by long-lived resonances, evidenced by the sharp oscillatory features. Due to its exothermic nature, the forward reaction has larger reactivity than the reverse reaction. A clear reaction threshold can be found near a collision energy of ~ 0.25 eV, thanks to the entrance channel barrier shown in Fig. 3. The clear modulation of the reaction probability with the collision energy at an interval of ~ 1000 cm^{-1} is likely due to the bottleneck states near the barrier,⁵⁷ although a more detailed investigation is needed. The situation is similar to that observed in our recent work on the $\text{O} + \text{O}_2$ exchange reaction.⁵⁸

The reaction probability for the reverse reaction is very small. The reaction threshold near 0.5 eV can be attributed to the endothermicity and the exit channel barrier. Additional partial waves need be included to obtain the experimentally measurable cross sections.

IV. Conclusions

In this work, we investigated the potential energy surface of the first excited (\tilde{A}^2A') state of HO_2 , using several high-level *ab initio* methods. The \tilde{A}^2A' -state PES features a deep well corresponding to a bent HO_2 . The global PES gives excellent

agreement with known thermodynamic and spectroscopic data on this system. Variational calculations on these PESs indicated however that the vibrational assignment in the literature needs modification. Scattering calculations indicate that the reaction R2 is dominated by long-lived resonances.

Acknowledgements:

The work at NJU was supported by the National Natural Science Foundation of China (20533060) and the Ministry of Science and Technology (2007CB815201). The Sandia and UNM teams were funded by Department of Energy (DE-FG02-05ER15694 to HG and DE-AC04-94-AL85000 to AWJ). Part of the calculations was carried out at the National Energy Research Scientific Computing (NERSC) Center.

References:

1. J. A. Miller, R. J. Kee and C. K. Westbrook, *Annu. Rev. Phys. Chem.* **41**, 345 (1990).
2. R. P. Wayne, *Chemistry of Atmospheres*. (Oxford University Press, Oxford, 2000).
3. M. S. Zahniser, K. E. McCurdy and A. C. Stanton, *J. Phys. Chem.* **93**, 1065 (1988).
4. M. A. Crawford, J. J. Szente and M. M. Maricq, *J. Phys. Chem. A* **101**, 5337 (1997).
5. J. D. DeSain, E. P. Clifford and C. A. Taatjes, *J. Phys. Chem. A* **105**, 3205 (2001).
6. A. M. Knepp, G. Meloni, L. E. Jusinski, C. A. Taatjes, C. Cavallotti and S. J. Klippenstein, *Phys. Chem. Chem. Phys.* **9**, 4315 (2007).
7. H. E. Hunziker and H. R. Wendt, *J. Chem. Phys.* **60**, 4622 (1974).
8. K. H. Becker, E. H. Fink, P. Langen and U. Schurath, *J. Chem. Phys.* **60**, 4623 (1974).
9. R. P. Tuckett, P. A. Freedman and W. J. Jones, *Mole. Phys.* **37**, 379 (1979).
10. E. H. Fink and D. A. Ramsey, *J. Mole. Spectrosc.* **184**, 304 (1997).
11. E. Renner, *Z. Phys.* **92**, 172 (1934).
12. G. Osmann, P. R. Bunker, P. Jensen, R. J. Buenker, J. Gu and G. Hirsch, *J. Mole. Spectrosc.* **197**, 262 (1999).
13. P. Jensen, R. J. Buenker, J. Gu, G. Osmann and P. R. Bunker, *Can. J. Phys.* **79**, 641 (2001).
14. V. V. Melnikov, T. E. Odaka, P. Jensen and T. Hirano, *J. Chem. Phys.* **128**, 114316 (2008).
15. V. V. Melnikov, P. Jensen and T. Hirano, *J. Chem. Phys.* **130**, 224105 (2009).
16. E. H. Fink and D. A. Ramsey, *J. Mole. Spectrosc.* **216**, 322 (2002).
17. M. M. Graff and A. F. Wagner, *J. Chem. Phys.* **92**, 2423 (1990).
18. H. Du and J. P. Hessler, *J. Chem. Phys.* **96**, 1077 (1992).
19. K. Kessler and K. Kleinermanns, *J. Chem. Phys.* **97**, 374 (1992).
20. A. I. Maergoiz, E. E. Nikitin, J. Troe and V. G. Ushakov, *J. Chem. Phys.* **108**, 5265 (1998).
21. E. M. Goldfield and A. J. H. M. Meijer, *J. Chem. Phys.* **113**, 11055 (2000).
22. S. Y. Lin, Z. Sun, H. Guo, D. H. Zhang, P. Honvault, D. Xie and S.-Y. Lee, *J. Phys. Chem. A* **112**, 602 (2008).
23. F. Lique, M. Jorfi, P. Honvault, P. Halvick, S. Y. Lin, H. Guo, D. Q. Xie, P. J. Dagdigian, J. Klos and M. H. Alexander, *J. Chem. Phys.* **131**, 221104 (2009).
24. A. Khchatrian and P. J. Dagdigian, *Chem. Phys. Lett.* **415**, 1 (2005).
25. I. W. M. Smith, *J. Chem. Soc. Faraday Trans.* **93**, 3741 (1997).
26. J. A. Klos, P. J. Dagdigian and M. Alexander, *J. Chem. Phys.* **129**, 064306 (2008).
27. B. Kendrick and R. T. Pack, *J. Chem. Phys.* **102**, 1994 (1995).
28. C. Xu, D. Xie, D. H. Zhang, S. Y. Lin and H. Guo, *J. Chem. Phys.* **122**, 244305 (2005).
29. G. Herzberg, *Molecular Spectra and Molecular Structure, Vol. 1, Spectra of Diatomic Molecules*. (Van Nostrand, Princeton, 1950).
30. A. B. MOLPRO is a package of ab initio programs written by H.-J. Werner and P.J. Knowles with contributions from R. D. Amos, D. L. Cooper, M. J. O. Deegan, A. J. Dobbyn, F. Eckert, C. Hampel, T. Leiginger, R. Lindh, A. W. Lloyd, W. Meyer, M. E. Mura, A. Nicklass, P. Palmieri, K. A. Peterson, R. Pitzer, P. Pulay, M. Schutz, H. Stoll, A. J. Stone, T. Thorsteinsson, (unpublished).

31. R. Dawes, D. L. Thompson, A. F. Wagner and M. Minkoff, *J. Chem. Phys.* **128**, 084107 (2008).
32. R. Dawes, D. L. Thompson, A. F. Wagner and M. Minkoff, *J. Phys. Chem. A* **113**, 4709 (2009).
33. M. P. Deskevich, D. J. Nesbitt and H.-J. Werner, *J. Chem. Phys.* **120**, 7281 (2004).
34. R. Dawes, A. W. Jasper, T. C., C. Richmond, C. Mukarakate, S. H. Kable and S. A. Reid, *J. Phys. Chem. Lett.* **1**, 641 (2010).
35. H.-J. Werner and P. J. Knowles, *J. Chem. Phys.* **89**, 5803 (1988).
36. P. J. Knowles and H.-J. Werner, *Chem. Phys. Lett.* **145**, 514 (1988).
37. S. R. Langhoff and E. R. Davidson, *Int. J. Quant. Chem.* **8**, 61 (1974).
38. T. Helgaker, P. Jorgensen and J. Olsen, *Molecular Electronic Structure Theory*. (Wiley, New York, 2000).
39. T. H. Dunning, *J. Chem. Phys.* **90**, 1007 (1989).
40. H.-J. Werner and P. J. Knowles, *Theo. Chem. Acc.* **78**, 175 (1990).
41. C. Xu, D. Xie, P. Honvault, S. Y. Lin and H. Guo, *J. Chem. Phys.* **127**, 024304 (2007).
42. B. Fu, X. Xu and D. H. Zhang, *J. Chem. Phys.* **129**, 011103 (2008).
43. J. Echave and D. C. Clary, *Chem. Phys. Lett.* **190**, 225 (1992).
44. H. Wei and T. Carrington Jr., *J. Chem. Phys.* **97**, 3029 (1992).
45. J. V. Lill, G. A. Parker and J. C. Light, *J. Chem. Phys.* **85**, 900 (1986).
46. C. Lanczos, *J. Res. Natl. Bur. Stand.* **45**, 255 (1950).
47. S. Y. Lin and H. Guo, *Phys. Rev. A* **74**, 022703 (2006).
48. Z. Sun, H. Guo and D. H. Zhang, *J. Chem. Phys.* **132**, 084112 (2010).
49. S. K. Gray and G. G. Balint-Kurti, *J. Chem. Phys.* **108**, 950 (1998).
50. Z. Sun, S.-Y. Lee, H. Guo and D. H. Zhang, *J. Chem. Phys.* **130**, 174102 (2009).
51. S. Gomez-Carrasco and O. Roncero, *J. Chem. Phys.* **125**, 054102 (2006).
52. V. A. Mandelshtam and H. S. Taylor, *J. Chem. Phys.* **103**, 2903 (1995).
53. B. Ruscic, R. E. Pinzon, M. L. Morton, N. K. Srinivasan, M. C. Su, J. W. Sutherland and J. V. Michael, *J. Phys. Chem. A* **110**, 6592 (2006).
54. R. P. Tuckett, P. A. Freedman and W. J. Jones, *Mole. Phys.* **37**, 403 (1979).
55. M. E. Jacox, *J. Phys. Chem. Ref. Data* **32**, 1 (2003).
56. K. J. Holstein, E. H. Fink and F. Zabel, *J. Mole. Spectrosc.* **99**, 231 (1983).
57. R. T. Skodje and X. Yang, *Int. Rev. Phys. Chem.* **23**, 253 (2004).
58. Z. Sun, L. Liu, S. Y. Lin, R. Schinke, H. Guo and D. H. Zhang, *Proc. Natl. Acad. Sci. USA* **107**, 555 (2010).
59. L. B. Harding, A. I. Maergoiz, J. Troe and V. G. Ushakov, *J. Chem. Phys.* **113**, 11019 (2000).
60. L. B. Harding, J. Troe and V. G. Ushakov, *Phys. Chem. Chem. Phys.* **2**, 631 (2000).
61. K. G. Lubic, T. Amano, H. Uehara, K. Kawaguchi and E. Hirota, *J. Chem. Phys.* **81**, 4826 (1984).

Table I: Numerical parameters used in the scattering calculations. (Atomic units used unless specified explicitly)

	H+O ₂ →O+OH	O+OH→H+O ₂
Grid/basis ranges and sizes	$R \in (0.1, 14.5)$, ($N_R=119$) $r \in (0.5, 14.5)$, ($N_r=335$) $\gamma \in (0, 90^\circ)$, $j=0-j_{\max}=88$, ($N_\theta = 45$)	$R \in (0.1, 15.0)$, ($N_R=335$) $r \in (0.5, 15.2)$, ($N_r=119$) $\gamma \in (0, 180^\circ)$, $j=0-j_{\max}=139$, ($N_\theta = 140$)
Position of final state projection	$\square'_{\infty}=8.0$	$\square'_{\infty}=8.0$
Damping ($x=r, R$) $\square\square=I$ $\square\square\square$ $\square \leq \square\square, \square - \square\square (\square - \square\square)^2$ $\square\square\square \square > \square\square.$	$R_d = 10.0, d_R = 0.005$ $r_d = 10.0, d_r = 0.01$	$R_d = 10.5, d_R = 0.005$ $r_d = 10.5, d_r = 0.01$
Initial wave packet: $e^{-((R-R_{i0})/\delta)^2/2} \cos(k_{i0}R)$	$R_{i0}=9.9$ $E_{i0} = \frac{\hbar^2 k_{i0}^2}{2\mu} = 0.4 \text{ eV}$ $\delta = 0.1$	$R_{i0}=9.9$ $E_{i0} = \frac{\hbar^2 k_{i0}^2}{2\mu} = 0.4 \text{ eV}$ $\delta = 0.1$
Spectral range	Energy cut of 0.2 Hartree for both potential and rotational kinetic energy terms.	Energy cut of 0.2 Hartree for both potential and rotational kinetic energy terms.
Propagation steps	30,000	28,000

TABLE II. Comparison of *ab initio* and experimental results for the equilibrium geometry and dissociation energies (in kcal/mol) for the $\tilde{X}^2 A''$ and $\tilde{A}^2 A'$ states of the HO₂

		$R_e(\text{OO})/a_0$	$R_e(\text{OH})/a_0$	θ_e/deg	$D_0(\text{H-OO})$	$D_0(\text{O-OH})$
$\tilde{X}^2 A''$	Harding <i>et al.</i> ⁵⁹⁻⁶⁰	2.532	1.853	103.6	44.4	60.6
	XXZLG ²⁸	2.521	1.836	104.12	47.36	62.69
	This work	2.515	1.831	104.25	47.66	63.56
	Expt.	2.514 ⁶¹	1.834 ⁶¹	104.29 ⁶¹	47.99±0.06 ⁵³	64.23±0.08 ⁵³
$\tilde{A}^2 A'$	Jensen <i>et al.</i> ¹³	2.651	1.818	100.0		
	Melnikov <i>et al.</i> ¹⁴	2.643	1.828	101.81		
	This work (PES1-1)	2.634	1.823	102.06		
	This work (PES1-2)	2.636	1.831	101.05		
	This work (PES1-3)	2.635	1.824	102.37		
	This work (PES2)	2.642	1.827	101.80	50.18	43.51
	Expt.	2.633 ⁵⁴	1.823 ⁵⁴	102.69 ⁵⁴	50.39*	44.13*
		2.668 ¹⁶	1.778 ¹⁶	95.36 ¹⁶		

*Estimated from ground state and spectroscopic data:

$$D_0(\text{O-OH}, \tilde{A}^2 A') = D_0(\text{O-OH}, \tilde{X}^2 A'') - T_0(\tilde{A}^2 A' \rightarrow \tilde{X}^2 A'')$$

$$D_0(\text{H-OO}, \tilde{A}^2 A') = D_0(\text{H-OO}, \tilde{X}^2 A'') + T_0(\text{O}_2(a^1\Delta_g) \rightarrow \text{O}_2(X^3\Sigma_g^-)) - T_0(\tilde{A}^2 A' \rightarrow \tilde{X}^2 A'')$$

TABLE III Geometries and energies for four stationary points of the HO₂ ($\tilde{A}^2 A'$) PES (PES2). Energies are relative to the minimum of HO₂.

	$R(\text{OO})/a_0$	$R(\text{OH})/a_0$	θ/deg	V/eV
Hydrogen-bonded OH-O minimum	5.929	1.835	0.0	1.923
Saddle point for O+OH	5.246	1.834	95.8	1.959
van der Waals H-O ₂ minimum	2.303	6.186	180.0	2.433
Saddle point for H+O ₂	2.304	4.422	58.6	2.712

TABLE IV. Calculated vibrational energy level (in cm^{-1}) of HO_2 ($\tilde{A}^2 A'$) for total angular momentum $J=0$ and comparison with experimental band origins.

(n_1, n_2, n_3)	This work (PES1-1)	This work (PES1-2)	This work (PES1-3)	This work (PES2)	Expt. ⁵⁵
(0,0,0)	2954.0	2888.5	2922.4	???	
(0,0,1)	932.2	929.7	938.1	928.0	929.068
(0,1,0)	1228.6	1217.8	1197.5	1196.2	1285
(0,0,2)	1854.9	1840.6	1857.6	1837.8	
(0,1,1)	2139.5	2128.9	2121.8	2110.2	
(0,2,0)	2402.8	2417.6	2379.6	2374.5	
(0,0,3)	2760.9	2733.0	2757.9	2728.8	
(0,1,2)	3044.8	3024.9	3028.1	3006.8	
(0,2,1)	3302.2	3308.1	3288.2	3273.6	
(0,3,0)	3553.7	3510.1	3542.6	3534.4	
(1,0,0)	3579.7	3587.2	3565.0	3566.7	3268.5
(0,0,4)	3645.0	3604.7	3638.5	3599.3	
(0,1,3)				3885.0	
(0,2,2)				4156.2	
(0,3,1)				4417.4	
(0,0,5)				4449.2	
(1,0,1)				4492.0	
(0,4,0)				4675.1	
(1,1,0)				4731.4	
(0,1,4)				4743.1	

Figure captions:

Figure 1. Contours of the $\text{HO}_2(\tilde{A}^2 A')$ PES in internal coordinates. Upper panel: contour plots at $\theta = 101.8^\circ$; lower panel: contour plots at $r_{\text{OH}} = 1.827 a_0$. The energy zero is defined at the $\text{HO}_2(\tilde{A}^2 A')$ minimum and contours are spaced by 0.3 eV.

Figure 2. Long-range behaviors of the $\text{HO}_2(\tilde{A}^2 A')$ PES. Upper panel: contour plot of the O+OH channel in the Jacobi coordinates with the OH bond length (r) fixed at its equilibrium $1.83 a_0$. The energy zero is defined at the OH+O dissociation limit and contour interval is 0.02 eV. Lower panel: contour plot of the H + O₂ channel in the Jacobi coordinates with the O₂ bond length (r) fixed at its equilibrium $2.30 a_0$. The energy zero is defined at the H + O₂ dissociation limit and contour interval is 0.1 eV.

Figure 3. Minimal energy paths for the H + O₂ (upper panel) and O + OH(lower panel) dissociation channels on the $\text{HO}_2(\tilde{A}^2 A')$ PES. The energy zero is defined at the O + OH asymptote.

Figure 4. Contour plots of nine vibrational states of $\text{HO}_2(\tilde{A}^2 A')$ in internal coordinates. Three vibrational quantum numbers (n_1 , n_2 , and n_3) represent the OH stretching, HOO bending, and O₂ stretching modes, respectively.

Figure 5. $J=0$ reaction probabilities for the forward and reverse R1 reactions as functions of the collision energy.

Figure 1

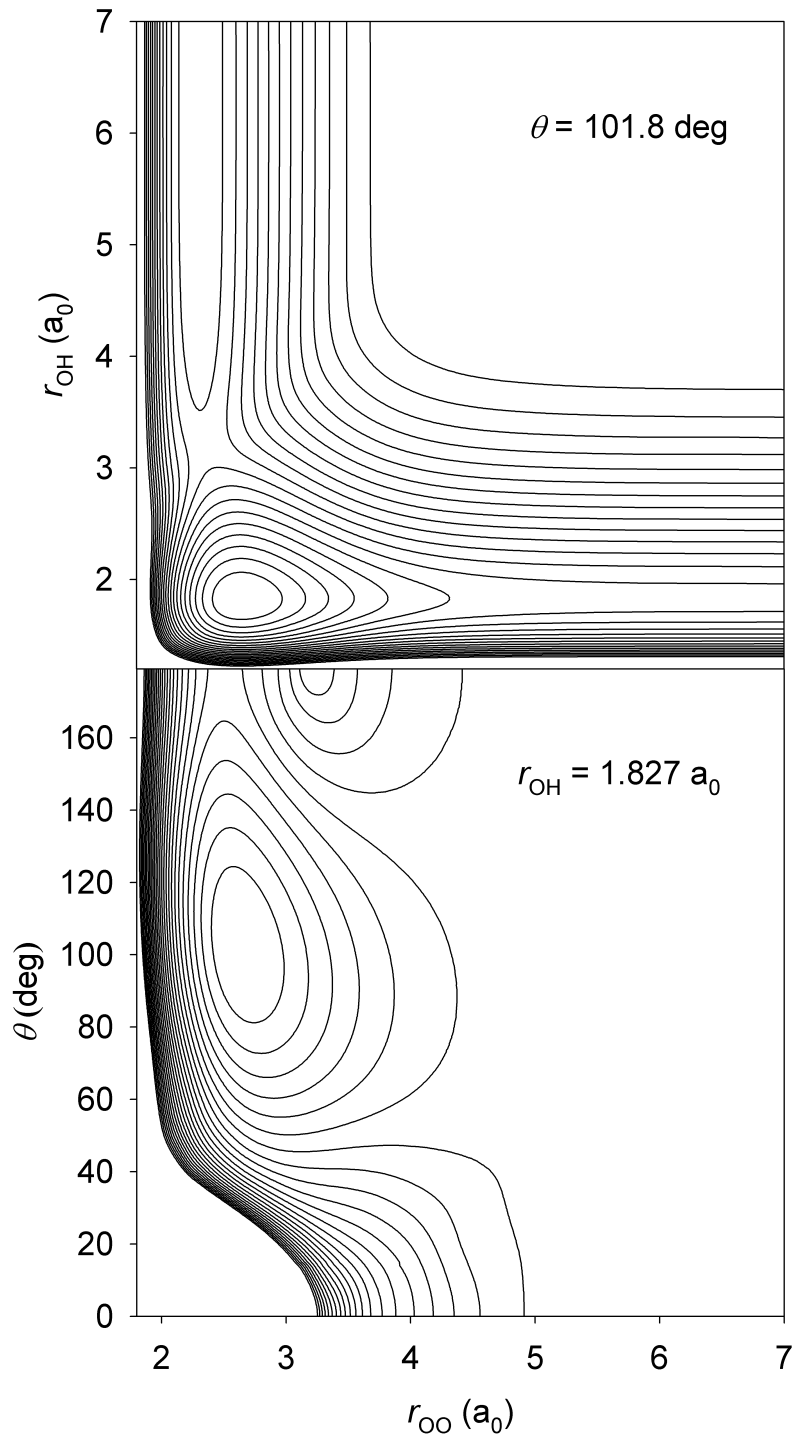


Figure 2

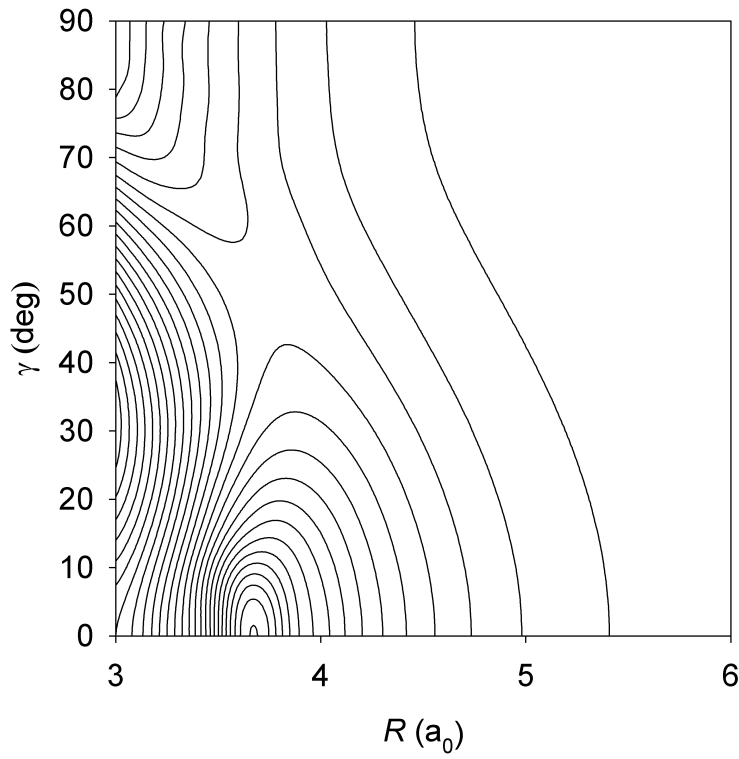
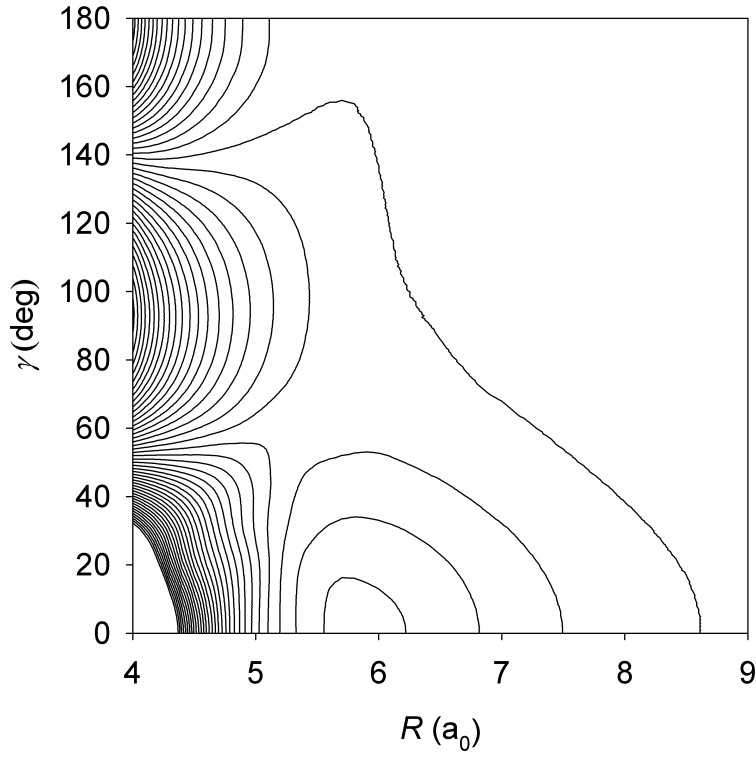


Figure 3

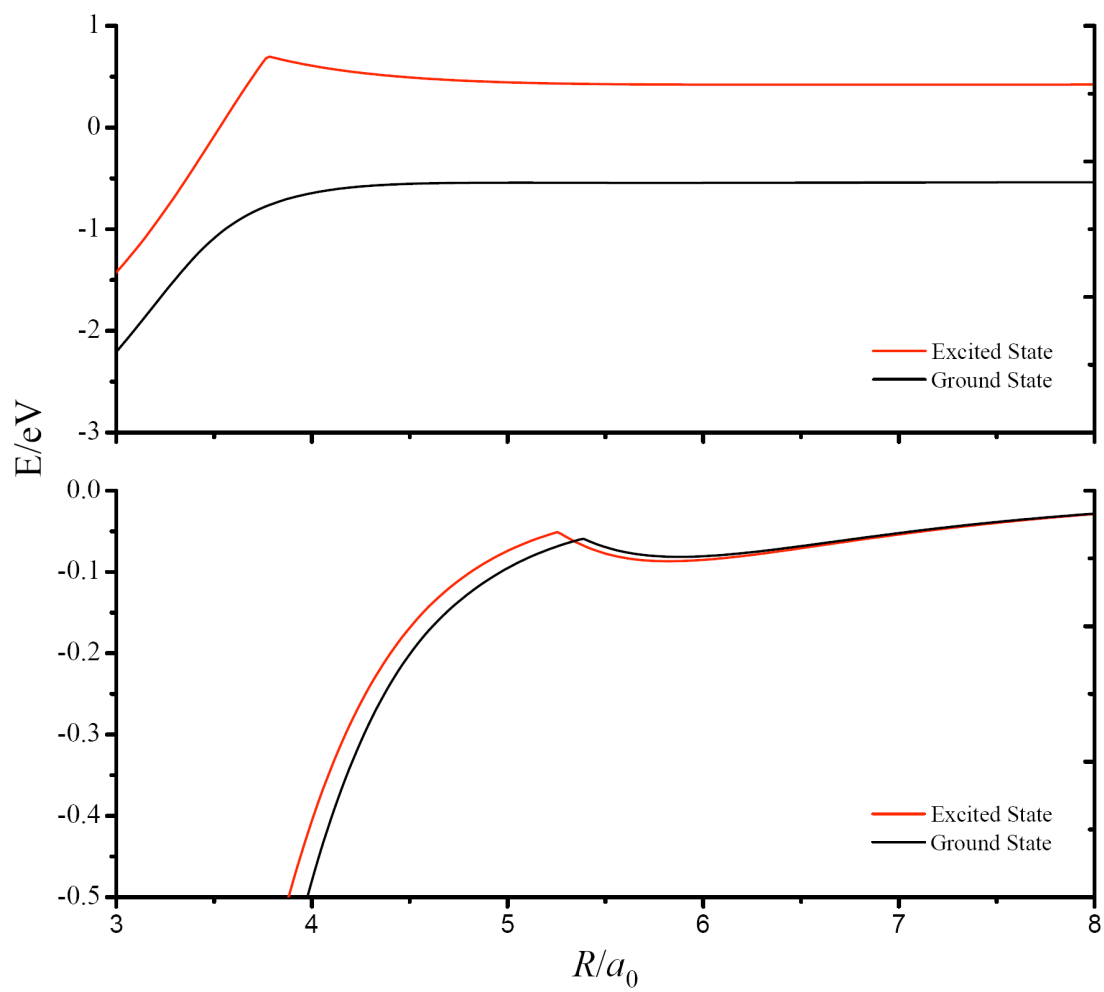


Figure 4

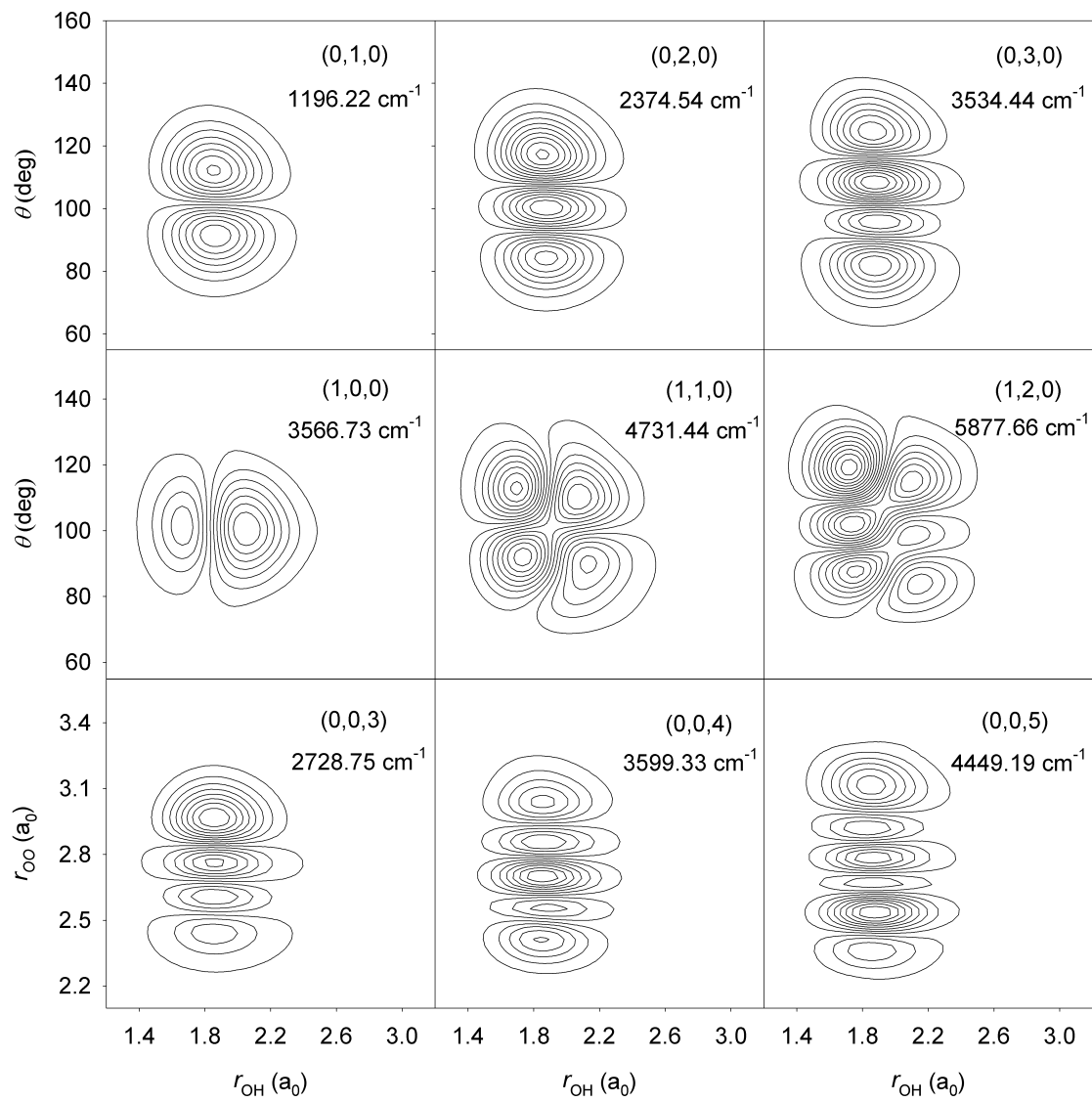


Figure 5

